

Nondestructive Evaluation Techniques for Development and Characterization of Carbon Nanotube Based Superstructures

Buzz Wincheski^{1, a)}, Jae-Woo Kim², Godfrey Sauti², Elliot Wainwright³, Phillip Williams¹, and Emile J. Siochi¹

¹NASA Langley Research Center, Hampton VA, 23681

²National Institute of Aerospace, Hampton VA, 23681

³The College of Wooster, Wooster OH, 44691

^{a)}Corresponding author: russell.a.winchkeski@nasa.gov

Abstract. Recently, multiple commercial vendors have developed capability for the production of large-scale quantities of high-quality carbon nanotube sheets and yarns [1]. While the materials have found use in electrical shielding applications, development of structural systems composed of a high volume fraction of carbon nanotubes is still lacking [2]. A recent NASA program seeks to address this by prototyping a structural nanotube composite with strength-to-weight ratio exceeding current state-of-the-art carbon fiber composites. Commercially available carbon nanotube sheets, tapes, and yarns are being processed into high volume fraction carbon nanotube-polymer nanocomposites. Nondestructive evaluation techniques have been applied throughout this development effort for material characterization and process control. This paper will report on the progress of these efforts, including magnetic characterization of residual catalyst content, Raman scattering characterization of nanotube diameter, defect ratio, and nanotube strain, and polarized Raman scattering for characterization of nanotube alignment.

INTRODUCTION

The use of carbon nanotube based materials for structural applications continues to be rare in spite of the astonishing material properties of individual carbon nanotubes. Cost, availability, and processing difficulties have limited most work to the development of low volume fraction carbon nanotube-polymer composites. While even a low volume fraction of carbon nanotubes has been found to be beneficial in increasing conductivity and strength compared to the neat polymers, structural properties have yet to approach those of state-of-the-art carbon fiber based composites.

Recently, an approach to the development of high volume fraction nanotube composites was demonstrated and shown to yield mechanical properties competitive with carbon fiber composites [3]. This work capitalized on a nanotube synthesis technique that produces large quantities of high-purity entangled carbon nanotubes in sheet and yarn formats [4]. Commercially available from Nanocomp Technologies, Inc., the nanotube materials are fabricated using a continuous floating catalyst chemical vapor deposition technique wherein a carbon fuel source and iron catalyst are continuously added at one end of the reactor and a carbon nanotube web is continuously produced at the other end. The nanotube web is condensed on a conveyor belt or captured on a spindle to create nanotube sheets and yarns, respectively. NASA is investigating techniques to use these materials as a starting point to produce a

structural nanotube composite with strength-to-weight ratio exceeding current state-of-the-art carbon fiber composites.

The development of these nanomaterial-based superstructures relies upon characterization of the nanotube starting material as well as quantification of relevant parameters during composite processing. In this work, nondestructive evaluation techniques, including magnetic characterization and in-situ polarized Raman scattering, are presented as a means to quantify residual catalyst content, nanotube alignment, and strain transfer in macroscale systems composed of a high volume fraction of individual carbon nanotubes.

RESIDUAL CATALYST CHARACTERIZATION

A side effect of the aforementioned technique to create nanotube sheets and yarns is that nanoscale catalyst particles, typically coated in an amorphous carbon shell, become embedded in the nanotube product. While purification steps can be pursued to remove the catalyst in post-processing, they are typically costly, time consuming, and potentially damaging to the carbon nanotubes themselves [5]. In addition, the particles can provide entanglement points to increase the load transfer between individual nanotubes in the superstructure. A small but non-zero quantity of these particles may thereby be beneficial in achieving optimal mechanical properties in a structural nanotube composite. As such, a detailed characterization of the percentage and size of the catalyst particles in the nanotube sheets and yarns is critical to understanding and optimizing the mechanical properties of the resultant nanotube superstructure. As catalyst sources for nanotube growth are typically iron based, a simple method for characterizing the catalyst involves the magnetic signature of the resulting carbon nanotube material [6].

Figure 1 shows SQUID magnetometry results at 300 kelvin for three carbon nanotube source materials: a carbon nanotube tape, a low-density carbon nanotube yarn, and a high-density carbon nanotube yarn. The data, summarized in Table 1, show that the magnetic properties of the three samples vary widely. The residual iron catalyst content can be estimated by dividing the saturation magnetization of the sample by that of pure iron, 218 emu/g. This gives a value of 7.9% by weight of Fe catalysts in the low-density yarn but only 3.7% in the high-density yarn. Also, the

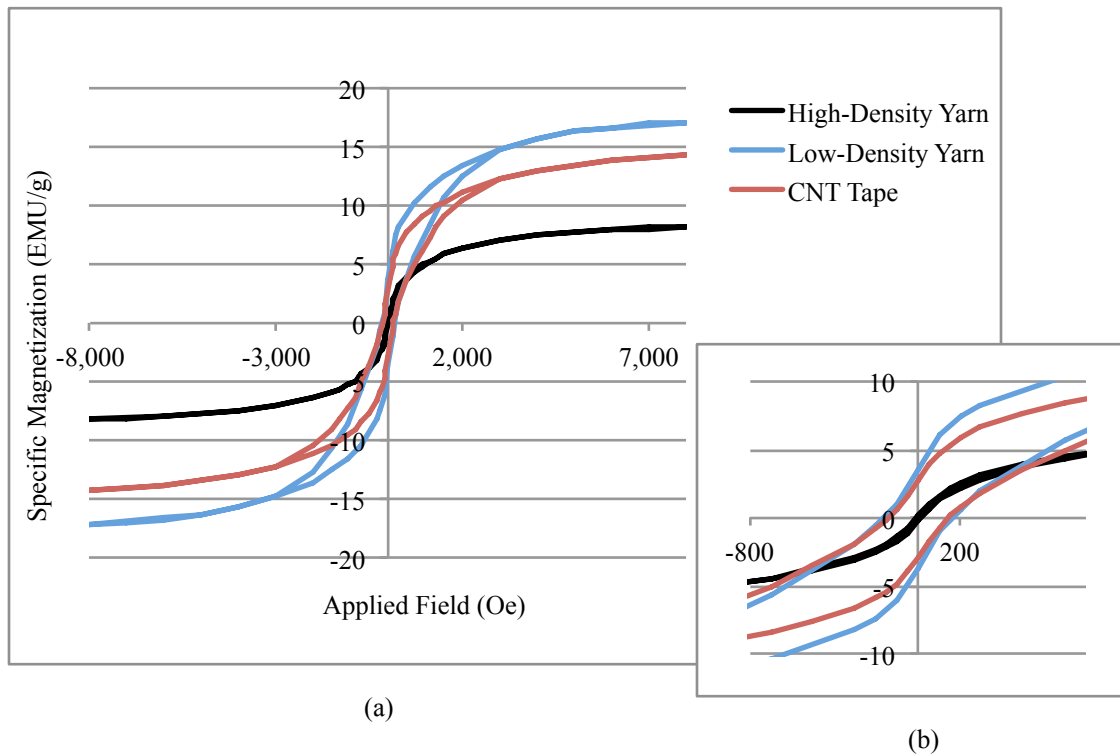


FIGURE 1. Hysteresis loops from three different carbon nanotube source materials. (a) Full loops show change in specific magnetization directly related to weight percent of residual catalyst. (b) Changes in coercive force prove insight into the size of residual catalyst particles.

coercivities of the samples are markedly different. The CNT tape and low-density yarn show a high coercive force associated with small-diameter, potentially single-domain, Fe particles. The high-density yarn, however, has very little coercivity. It is believed that the size of the iron particles in the high-density yarn is beneath the critical diameter D_p for stable magnetic domains to form at 300 kelvin [7]. It is known that different reactor conditions are used in the growth of the different nanotube sources, and those varying conditions are likely the cause of the different magnetic signatures of the samples. The magnetic technique demonstrated here could prove useful in quality control of the nanotube sources as well as in process monitoring and optimization of the reactor conditions during nanotube growth.

Table 1. Magnetic Properties of Various Carbon Nanotube Material Formats

Material Under Test	Saturation Magnetization (emu/g)	Coercive Force (Oe)	Remanence (emu/g)
Nanotube Tape	14.2	138	2.74
Low-Density Yarn	17.2	162	3.65
High-Density Yarn	8.17	< 10	< 0.2

CARBON NANOTUBE ALIGNMENT AND STRAIN MEASUREMENTS

Individual carbon nanotubes are known to have exceptional mechanical properties along the axis of the nanotube with theoretical ultimate strength and elastic modulus as high as 100 GPa and 1000 GPa, respectively. While it is anticipated that a knock-down from these nanoscale properties will result during the scale-up to a macroscopic material, material processing steps are being designed with the goal of minimizing this knock-down. Two important factors that reduce macroscopic properties as compared to those at the nanoscale are alignment of the nanotubes along the stress axis and strain transfer between individual nanotubes in the superstructure. Raman spectroscopy provides an experimental technique for the nondestructive monitoring of these two important processing parameters.

Raman spectroscopy is a technique in which vibrational modes of a crystal or molecule are excited by the inelastic scattering of light. Typically, a narrow-wavelength laser source is directed at the material under test. As the photons impinge on the sample, a vibrational (phonon) mode of the crystal can be excited, leading to a loss of energy of the light that is equivalent to the energy of the excited phonon mode. The scattered and reflected light is collected by a spectrometer, and the wavelength spectrum measured. The Raman spectrum is then plotted as intensity versus Raman shift where the Raman shift is defined as

$$\Delta w = (1/\lambda_0 - 1/\lambda_1). \quad (1)$$

Here, Δw is the Raman shift (typically reported in units of cm^{-1}), λ_0 is the excitation wavelength, and λ_1 is the wavelength of the scattered light.

Figure 2 displays the Raman spectrum acquired on a carbon nanotube sheet. The data were acquired using a Kaiser Raman RXN1TM Microprobe configured with a 785 nm laser at 100 mW output power. The prominent peak at $\sim 1580 \text{ cm}^{-1}$ is related to the C-C bond stretching between the two dissimilar carbon atoms in the graphene unit cell. Commonly referred to as the G band, this peak in a carbon nanotube consists of two sub components, G^+ and G^- , associated with vibrations along the nanotube axis (longitudinal optical phonon mode) and vibrations along the circumferential direction of the nanotube (transverse optical phonon mode), respectively [8]. The second strongest peak in the Raman spectrum of Fig. 2 occurs at $\sim 1350 \text{ cm}^{-1}$ and is a disorder-induced mode (so-called D band) involving elastic phonon scattering from a defect site [9]. The ratio of the intensity of the disorder-induced D band at 1350 cm^{-1} to that of the G band can be used as a measure of nanotube quality in the material. The two other prominent features in the Raman spectrum of Fig. 2 occur at approximately 2700 cm^{-1} and near 250 cm^{-1} . The strong peak near 2700 cm^{-1} is alternatively referred to as the G' peak (being a strong symmetry allowed peak in perfect graphite crystals) or the 2D peak (being an overtone of the D peak) [9]. Like the D peak, it arises from a second-order process involving phonon scattering. In the 2D (G') peak, the process involves a double-resonance scattering by two phonons as opposed to a phonon and defect as described above for the D band [9]. The set of

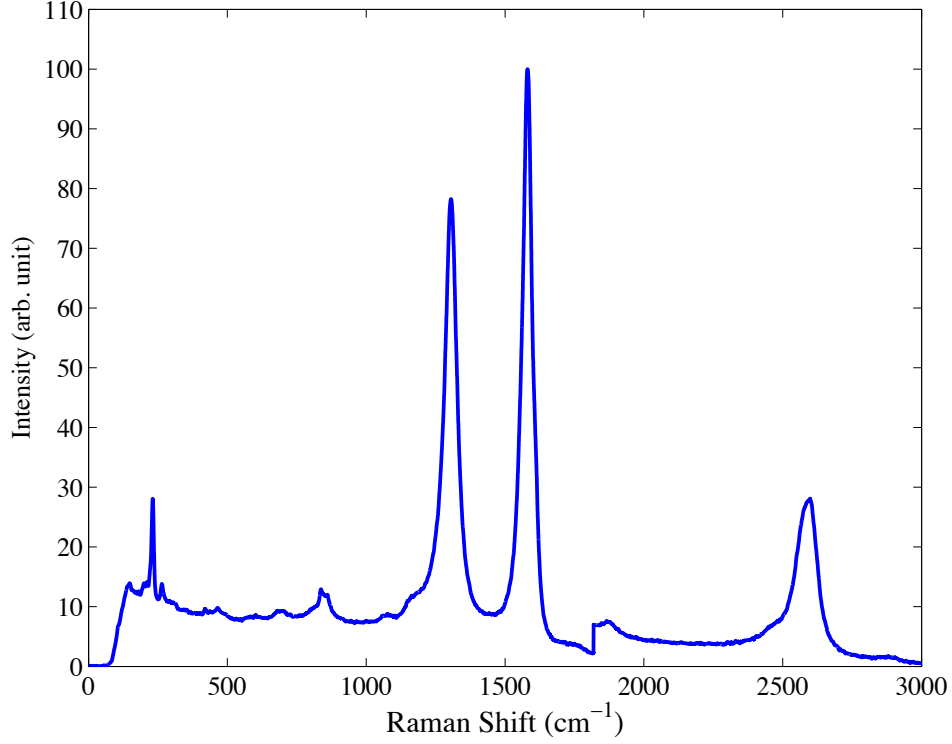


FIGURE 2. Raman spectrum for carbon nanotube sheet.

peaks near 250 cm^{-1} are a result of radial breathing modes (RBM) of the single walled nanotubes in the sample. The RBM, like the G mode, is a first order Raman process. In the RBM all carbon atoms move coherently in the radial direction [8]. The wavenumber of this mode is inversely proportional to the diameter of the single wall carbon nanotube being interrogated and is often used to calculate this quantity.

Polarized Raman spectroscopy has been shown as a method to characterize the alignment of individual nanotubes in nanotube based fibers, thin films, and composites [10-12]. As shown by Zamora et al., the orientation distribution of the nanotubes can be described by the three-dimensional order parameter S ,

$$S = \frac{1}{2} \langle 3 \cos^2 \beta - 1 \rangle \quad (2)$$

where, β is the angle between the nanotube and the measurement axes. Using the approximation that the Raman polarization tensor is non-negligible only for incident and scattered light parallel to the nanotube axis allows equation (2) to be rewritten in terms of the Raman intensities under three different polarization conditions [11].

$$S = (3I_{VV} + 3I_{VH} - 4I_{HH}) / (3I_{VV} + 12I_{VH} + 8I_{HH}) \quad (3)$$

where, I_{VV} , I_{HH} , and I_{VH} are the Raman intensities for incident and reflected light polarized parallel, perpendicular, and cross polarized, respectively, with respect to the CNT alignment direction.

In our experimental configuration, light is directed at the sample along the Z-axis and linearly polarized along either the X or Y axes. The sample lies in the XY plane with nominal alignment along the X-axis. The back reflected light from the sample is collected along the Z'-axis and passes through a second X/Y polarizer before reaching the spectrometer. Three polarization configurations, $\langle ZXXZ' \rangle$, $\langle ZYYZ' \rangle$, and $\langle ZXYZ' \rangle$, are collected to calculate the order parameter as defined above. Following data acquisition, the Raman spectra are processed to isolate the G+ peak from the G band for each polarization configuration, and the intensities from these peaks are used as the inputs to equation (3).

Along with nanotube alignment, Raman scattering can be used to measure the strain on the individual nanotubes under test. The strain-induced changes in Raman spectra for individual and bundled carbon nanotubes have been previously studied [13, 14]. As a nanotube is strained, there is an elongation of the carbon-carbon bonds, weakening the bond strength. The weaker bond strength results in a drop in energy of the G+ band and therefore less loss in energy of the Raman scattered light. The wavelength of the scattered light decreases closer to that of the excitation source and, by equation (1), a downshift in the G+ band is detected. Experimental evaluation of this effect has shown a downshift of the G+ band of $27.9 \text{ cm}^{-1}/\%$ strain [13]. Assuming a CNT modulus of 1 TPa, this equates to a stress-induced downshift of $2.79 \text{ cm}^{-1}/\text{GPa}$ for the G+ band.

Apparatus for In-Situ Measurements of Nanotube Alignment and Strain

Figure 3 shows a solid model of a miniature load frame designed to study the strain-induced alignment of carbon nanotube materials as well as the strain transfer in a nanotube network. The system is designed to fit under the Raman microprobe described above while applying loads of up to 25 pounds to the material under test. The load frame is displacement-controlled by a stepper motor with minimum step size of $0.000125''$. The nominal gauge length of the samples was set to $0.75''$, resulting in a strain resolution of 167 micro-strain. A 25-pound load cell with accuracy of ± 0.0375 pounds was incorporated such that load – displacement curves of the material under test can be generated.

Experimental Results

Figure 4 displays experimental results for the dichroic ratio, I_{xx}/I_{yy} , and the G+ band shift with strain for a carbon nanotube sheet placed under uniaxial strain up to 24% along the X-axis. The relative alignment, measured by the dichroic ratio, increases nearly linearly with strain up to 13% strain, after which there is a step decrease in alignment followed by a continued slight decrease with increasing strain. The nanotube strain, measured by the downshift in the G+ band peak position, follows a similar trend. The G+ band position decreases with increasing strain to a maximum change of -3.16 wavenumbers at 11% strain.

During testing, the change in trending of the data at 16% strain was observed, and a second data set was acquired at this strain level to verify the results. Once the results were confirmed, the testing was continued up to a strain of 24%. At this point the sample was examined, while held at 24% strain, under the optical microscope on the Raman microprobe. The sample was scanned under the microscope using the sample stage driven by a stepper motor, and a failure site in the CNT sheet was observed, which is believed to have originated during the approach to 16% strain level. Under careful examination, it was found that the failure was not complete and that a strand of the CNT sheet bridged the tear in the material. An optical photograph of the failure site and fiber bridging the tear is shown in fig. 5.

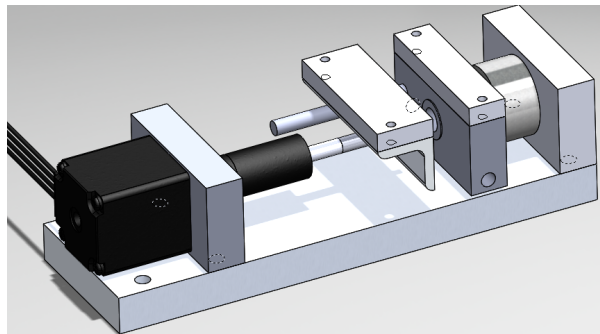


FIGURE 3. Apparatus for in-situ Raman measurements of CNT based materials under applied strain.

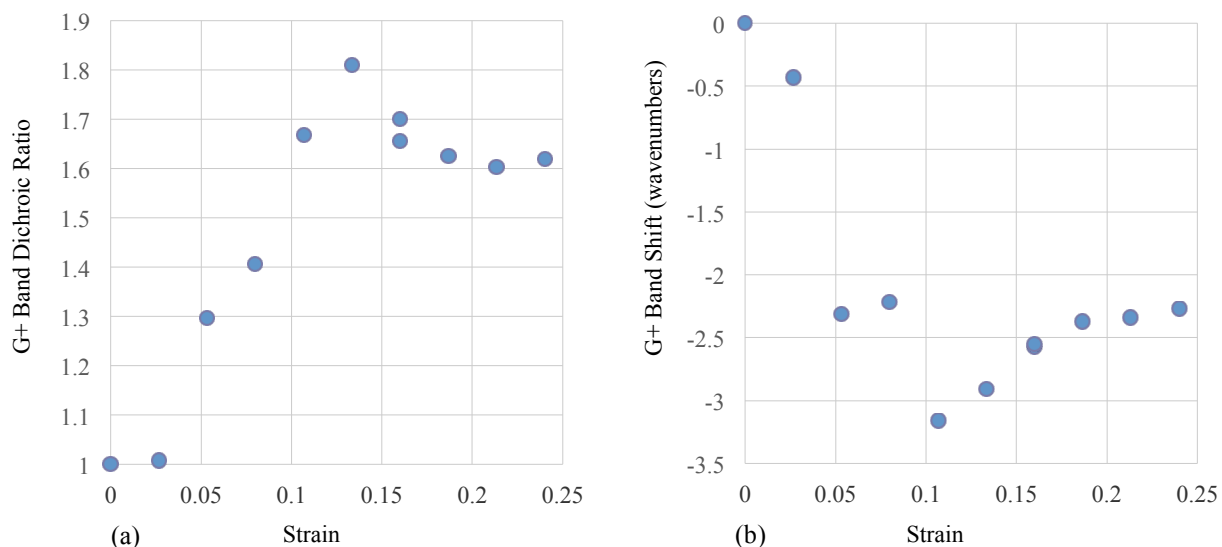


FIGURE 4. (a) Strain-induced changes in alignment measured by Raman dichroic ratio and (b) nanotube strain measured by shift in the G+ band position.

Analysis of the Raman signature of the fiber bridging the tear in the nanotube sheet shown in Fig. 5 verified an extremely high degree of strain-induced alignment and stress on the nanotube fiber. The dichroic ratio I_{xx}/I_{yy} was measured as 9.98, an increase of more than 5-fold over the peak ratio away from the damage. Analysis of the G+ band peak position showed a downshift of 10.75 cm^{-1} , which equates to a stress level of 3.85 GPa for the individual nanotubes entangled in the fiber.



FIGURE 5. Optical micrograph of fiber bridging tear in nanotube sheet. Cross hair in image indicates the area from which Raman spectroscopy data were acquired.

A final experimental study using the in-situ Raman load frame shown in Fig. 3 was performed to examine the effect of different carbon nanotube material formats and processing treatments on the alignment and nanotube strain transfer. Nanotube sheet material, supplied in tape format, and nanotube yarn material in both a low-density and high-density format were examined. In addition, the nanotube tapes were studied during a dry stretching process and during a solvent based stretching process in which the material was maintained in a methanol-wetted state during stretching. All processing of the yarn materials was performed under dry conditions. The results from this work are summarized in Table 2. In comparing the results of the three materials under dry stretching, it is apparent that the yarn material begins in a more aligned state and that strain-induced alignment has a smaller impact on the final order of the structure in the yarn based materials. This is because the processes used to produce the yarns involve drawing-out, consolidating and thus pre-aligning the carbon nanotube feed. While the order parameter of the tape was increased by more than 3 times, that of the high-density yarn was only increased by approximately 7%. Wetting of the material was found to increase the achievable alignment, but the load transfer between nanotubes was greatly reduced as indicated by the small wavenumber downshift of the wet stretch tape. The solvent wetting of the tape material during stretching possibly enabled an increase in the slippage of nanotubes past each other or an increase in the physical separation of the nanotubes within the material and thereby resulted in the observed reduction of load transfer between the nanotubes.

TABLE 2. Summary Data for Raman Analyses of Three Different Nanotube Material Formats

Material Under Test	Initial Raman Order Parameter	Maximum Raman Order Parameter Under Strain	Maximum Wavenumber Shift Under Strain
Dry Stretch Tape	0.05	0.16	2.3 cm ⁻¹
Wet Stretch Tape	0.05	0.20	0.9 cm ⁻¹
Low-Density Yarn	0.15	0.25	1.5 cm ⁻¹
High-Density Yarn	0.58	0.62	2.9 cm ⁻¹

SUMMARY

The development of ultra-lightweight materials and structures is embedded in several of the grand challenges facing NASA and can result in game-changing disruptive technology to enable new capabilities and missions. Carbon nanotube based structural materials are being studied as a potential technology to help meet these challenges. Incredibly strong at the nanoscale, nanotube based materials are beginning to show the capability to sustain several GPa level stresses at macroscopic lengths as evidenced by recent work. The ability of the nanotube based materials to sustain stresses of this magnitude shows that they can be competitive with state-of-the-art carbon fibers; however, continued research is required to determine the optimum nanotube starting material format and processing conditions to achieve an aerospace-grade carbon nanotube based structural material. In this work, a magnetic technique for residual catalyst characterization has been presented along with Raman spectroscopy based methods for characterization of nanotube alignment and strain transfer. The techniques are being utilized to perform material characterization and to optimize procedures with the goal of developing a structural nanotube composite with high strength-to-weight ratio exceeding current state-of-the-art carbon fiber composites.

REFERENCES

1. De Volder, M.F.L., et al., *Carbon nanotubes: present and future commercial applications*. Science, 2013. **339**(6119): p. 535-539.
2. Chou, T.-W., et al., *An assessment of the science and technology of carbon nanotube-based fibers and composites*. Composites Science and Technology, 2010. **70**(1): p. 1-19.

3. Cheng, Q., et al., *Functionalized carbon-nanotube sheet/bismaleimide nanocomposites: mechanical and electrical performance beyond carbon-fiber composites*. *Small*, 2010. **6**(6): p. 763-7.
4. Cheng, Q., et al., *High mechanical performance composite conductor: multi-walled carbon nanotube sheet/bismaleimide nanocomposites*. *Advanced Functional Materials*, 2009. **19**(20): p. 3219-3225.
5. Lin, Y., et al., *Purification of Carbon Nanotube Sheets*. *Advanced Engineering Materials*, 2014.
6. Sun, K.J., R.A. Wincheski, and C. Park, *Magnetic property measurements on single wall carbon nanotube polyimide composites*. *Journal of Applied Physics*, 2008. **103**(2).
7. Cullity, B.D., *Superparamagnetism in fine particles*, in *Introduction to Magnetic Materials*, M. Cohen, Editor. 1972, Addison-Wesley: Philippines. p. 410-418.
8. Dresselhaus, M.S., et al., *Raman spectroscopy of carbon nanotubes*. *Physics Reports*, 2005. **409**(2): p. 47-99.
9. Reich, S. and C. Thomsen, *Raman spectroscopy of graphite*. *Phil. Trans. R. Soc. Lond. A*, 2004. **362**: p. 2271-2288.
10. Anglaret, E., et al., *Raman resonance and orientational order in fibers of single-wall carbon nanotubes*. *Physical Review B*, 2002. **65**(16).
11. Zamora-Ledezma, C., et al., *Anisotropic thin films of single-wall carbon nanotubes from aligned lyotropic nematic suspensions*. *Nano Letters*, 2008. **8**(12): p. 4103-4107.
12. Zamora-Ledezma, C., C. Blanc, and E. Anglaret, *Orientational order of single-wall carbon nanotubes in stretch-aligned photoluminescent composite films*. *Physical Review B*, 2009. **80**(11): p. 113407.
13. Cronin, S.B., et al., *Measuring the uniaxial strain of individual single-wall carbon nanotubes: resonance raman spectra of atomic-force-microscope modified single-wall nanotubes*. *Physical Review Letters*, 2004. **93**(16): p. 167401.
14. Kumar, R. and S.B. Cronin, *Raman scattering of carbon nanotube bundles under axial strain and strain-induced debundling*. *Physical Review B*, 2007. **75**(15): p. 155421.